International Journal of Coal Science & Technology (2023) 10:34
https://doi.org/10.1007/s40789-023-00592-7

RESEARCH

Frictional behavior of quartz gouge during slide-hold-slide considering normal stress oscillation

Kang Tao[1] · **Wengang Dang**[1,2]

Received: 18 November 2022 / Revised: 7 February 2023 / Accepted: 9 May 2023

Abstract

Slide-hold-slide (SHS) test is an essential experimental approach for studying the frictional stability of faults. The origin SHS framework was established based on a consistent constant normal stress, which cannot truly reflect the stress disturbance around fault zones. In this paper, we conducted a series of 'dynamic SHS tests', which includes normal stress oscillations in the relaxation stage with different oscillation amplitudes and frequencies on synthetic quartz gouge using a double direct shear assembly. The experimental results reveal that the amplitude of the normal load oscillation has a remarkable effect on the frictional relaxation and healing patterns. However, the frequency of the normal load oscillation has a minor effect. Additionally, the shear loading rate is proportional to the normal loading rate during the relaxation stage, and the normal stiffness of the quartz layer remains nearly constant under various loading conditions. The creep rate during the hold phase is not obviously affected by the normal load oscillation, while the precursory slip is also sensitive to the oscillation amplitude. This study provides insights into the evolution of frictional stability in discontinuities and is beneficial for controlling relative disasters in fault zones.

Keywords Slide-hold-slide test · Normal load oscillation · Frictional healing · Fault stability

List of symbols

σ_n (MPa)	Normal stress
τ (MPa)	Shear stress
δ_h (mm)	Creep length that occurs during the hold
δ_p (mm)	Precursory slip
δ_s (mm)	Slip from reloading to reach the stable value of sliding friction
A (MPa)	Normal load oscillation amplitude
ε (–)	Normalized oscillation amplitude
f (s)	Normal load oscillation period
v_{lp} (mm/min)	Load point velocity
μ (–)	Apparent friction coefficient
μ_{ss} (–)	Friction coefficient of steady state
μ_{pk} (–)	Peak friction coefficient after the reload
μ_{min} (–)	Minimum friction coefficient during hold
$\Delta\mu_c$ (–)	Frictional relaxation
$\Delta\mu_w$ (–)	Frictional healing
β_c (–)	Relaxation rate
β_w (–)	Healing rate
Δu_c (mm)	Normal compaction
Δu_d (mm)	Normal displacement variation during one load cycle

✉ Wengang Dang
dangwg@mail.sysu.edu.cn

Kang Tao
touyasu@163.com

[1] School of Civil Engineering, Sun Yat-Sen University, Zhuhai 519086, China

[2] Southern Marine Science and Engineering Guangdong Laboratory, Zhuhai 519086, China

1 Introduction

Fault zones are commonly confronted in deep mining and geo-reservoir constructions. Seismogenic fault zones are comprehensive spatial–temporal regions, which are influenced by mineral types, fracture roughnesses and fluid lubrification (Carpenter et al. 2016a, 2016b; Ikari et al. 2009, 2014; Fang et al. 2018; Zhang et al. 2019, 2021; Jia et al. 2022), as well as different sliding velocities and strain rates in the seismic cycles (Beroza and Ide 2011; Ide et al. 2007; Fan et al. 2020). In-situ surveys showed that the fault zones are containing granular abrasive products, i.e., 'fault gouge' (Ikari et al. 2009, 2014; Carpenter et al. 2016b; Zhang et al. 2019). The range of gouge layers' widths can be millimeter-scale up to kilometer-scale (Montgomery and Jones 1992;

Published online: 20 June 2023

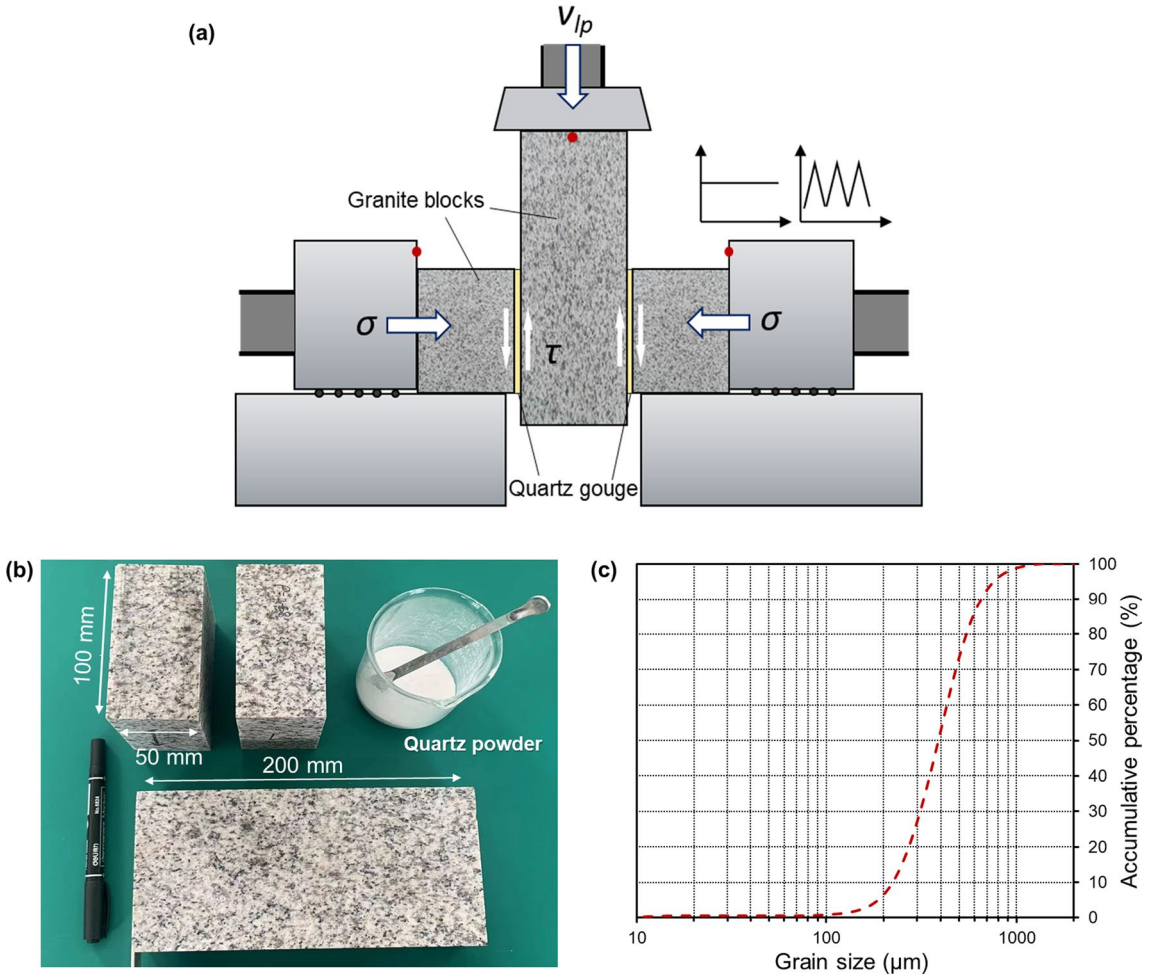

Fig. 1 Experimental configuration. **a** Experimental geometry and loading mode. Red dots are locations where the LVDTs attached **b** The photo of granite samples and infilled synthetic gouge **c** The grain size distribution of the quartz powder

Unsworth et al. 1997). Natural gouges mostly consist single or groups of phyllosilicate, tectosilicate, and carbonate minerals. Gouge containing tectosilicate minerals (like quartz) often exhibits relatively large shear strength (Blanpied et al. 1995; Zhang et al. 2019). The velocity-weakening behavior in tectosilicate-rich samples is widely detected and dynamic stick–slip events can occur under high normal stress level. On the contrary, phyllosilicate minerals such as talc, illite, chlorite, etc., usually present low frictional strength and have a positive contribution to velocity-strengthening effect causing aseismic slip (Saffer and Marone 2003; Carpenter et al. 2011). For carbonates, which are commonly found in crustal faults, illustrate complex frictional behavior depending on fluids, normal stress levels, sliding velocities, and thermal effects (Verberne et al. 2015; Carpenter et al. 2016b).

It is widely reported that the local movements on preexisting faults, disturbed by both human activities and tectonic effects, results in substantial seismic events (Xu et al. 2016; Foulger et al. 2018; Chen 2020; Harris 2017; Bürgmann 2018; Vlek 2018; Collettini et al. 2019). Mining, explosion, reservoir operation producing variable normal stress affect the natural fault zones, showing a variety of frictional patterns (van der Elst and Savage 2015; Delorey et al. 2017; Beeler et al. 2018; Li et al. 2022). Frictional response of rock fractures under dynamic normal load does not obey the traditional Amontons-Coulomb's law, showing a unique pattern (e.g., Kilgore et al. 2017; Dang et al. 2021, 2022a, 2022b). These tests revealed how the dynamic loads influence the frictional properties of long-time sliding fractures; however, the frictional properties will also be disturbed during the quasi-stationary contacts.

Faults are known to gain strength after activation, and the activation may then lead to strength loss (Dieterich 1972; Das and Aki 1977). Seismic data revealed that the decrease

Table 1 Test scheme. All the SHS tests were performed under normal stress level of 5 and 7 MPa

No.	Load point velocity (mm/min)	Normal load oscillation frequency (Hz)	Normalized normal load oscillation amplitude (%)	Oscillation amplitude of normal stress (MPa)
CH1	0.5	n/a	0	0
FH1	0.5	0.1	10	0.5, 0.7
FH2	0.5	0.2	10	0.5, 0.7
FH3	0.5	0.25	10	0.5, 0.7
FH4	0.5	0.5	10	0.5, 0.7
FH5	0.5	1.0	10	0.5, 0.7
AH1	0.5	0.5	5	0.25, 0.35
AH2	0.5	0.5	10	0.5, 0.7
AH3	0.5	0.5	15	0.75, 1.05
AH4	0.5	0.5	20	1.0, 1.4
AH5	0.5	0.5	25	1.25, 1.75

Test CH1 was executed without oscillatory loads. Tests FH1–FH5 concerned the effects of normal load oscillation frequency (from 0.1 to 1 Hz), and Test AH1–AH5 concerned the effects of normal load oscillation amplitude (from 5% to 25%)

of tectonic stress in seismic region increases logarithmically with time. Laboratory experiments on rock friction also demonstrated that the friction on static contact (after the yield strength of the friction surface) decreases logarithmically with time (Marone 1998a, 1998b; Marone and Saffer 2015; Im et al. 2017). The stabilities of frictional sliding systems are usually determined by slight variations in friction (induced by velocity or load changes) (Marone 1998a, 1998b; Dieterich and Kilgore 1994; McLaskey et al. 2012). To be specific, direct shear tests were performed using laboratory scale rock fractures (bare or infilled). When the shear stress reaches the yield value, the velocity at the loading point suddenly drops to zero. At this time ('hold stage', or 'relaxation stage'), the shear force still exists, but it will decline rapidly first and then slowly. After, the loading point velocity suddenly returned to its original value, and the laboratory fault would 'heal'.

This kind of test is referred as 'slide-hold-slide' (SHS) (Marone 1998b), which is regarded as a feasible model to simulate seismic cycles in nature. In many researches, SHS tests were performed considering the effects of gouge property, surface geometry, fluids, temperature, etc. (Ikari et al. 2014; Carpenter et al. 2016a, 2016b; Zhang et al. 2019; Fan et al. 2020; Jia et al. 2022). However, in previous researches, SHS tests were carried out under constant normal stress; thus, the role of stress disturbance during fault interseimic periods was little investigated. Therefore, we selected quartz as a representative gouge material to study the fault frictional stability. In this study, we performed one conventional SHS test and two sets of 'dynamic' SHS tests to reveal the role of dynamic stress disturbance in the seismic cycles of tectonic faults. The effects of normal load oscillation frequency, normal load oscillation amplitude and normal stress level during the hold stage were explored. This study provides new insights on the frictional behaviors of lithosphere discontinuities and is beneficial for relative disaster prevention of deep mining.

2 Experimental set-up

2.1 Apparatus and samples

All friction experiments were performed in double-direct shear configuration using a self-developed shear apparatus (DWZ-250) (Dang et al. 2022c, Fig. 1a). The test configuration consisted of two identical layers of simulated gouges sandwiched between three granite forcing blocks: a central block and two stationary side blocks (e.g. Marone 1998a; Zhang et al. 2019; Violay et al. 2021). Two hydraulic jacks in horizontal direction were used to apply loads normal to the granite, while a vertical hydraulic jack was used to apply shear load at designed shear rate. Loads were measured using load cells (accuracy ± 0.1 kN), positioned at the end of the ram, which is stiff enough and its self-deformation can be neglected. Horizontal displacements were measured by two LVDTs (linear variable differential transformers) with a resolution of ± 0.1 μm. The load point displacements were measured by a deformation sensor inserted in vertical piston, and the sliding distance was obtained from a vertical LVDT attached on the middle sliding block and its resolution was ± 0.1 μm.

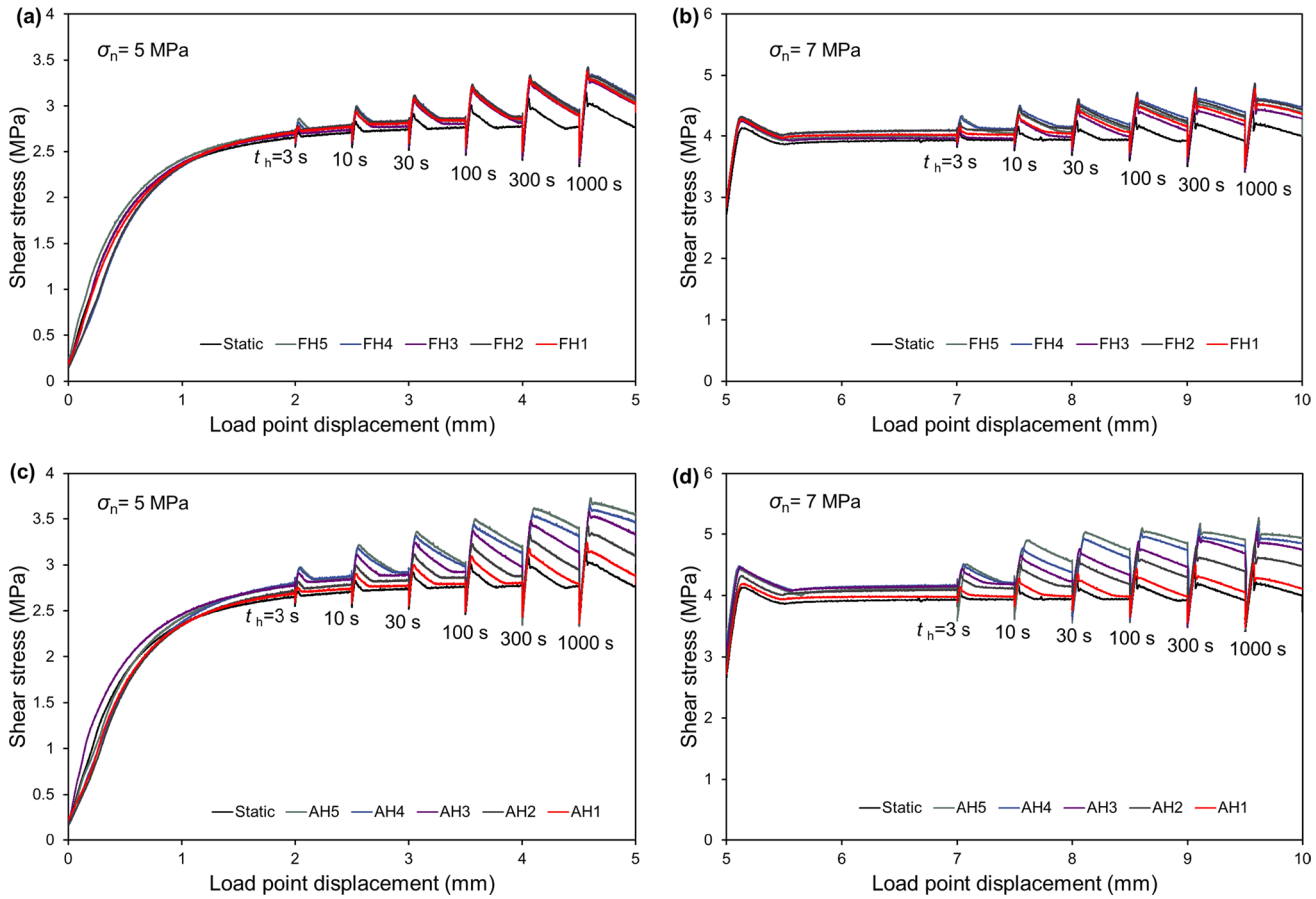

Fig. 2 Shear stress evolution of SHS tests. **a** Test FH1–FH5, $\sigma_n = 5$ MPa **b** Test FH1–FH5, $\sigma_n = 7$ MPa **c** Test AH1–AH5, $\sigma_n = 5$ MPa **d** Test AH1–AH5, $\sigma_n = 7$ MPa

The granite cubes in our experiment were sourced from Chinese Sichuan Province, and previous mechanical test showed its Young's modulus is 82.8 GPa, the tensile strength is 7.51 MPa, and the uniaxial compressive strength is 151.7 MPa. The sliding surfaces were created with diamond saw and were uniformly polished (Fig. 1b). The length of the central sliding rock and two stationary blocks was 200 mm and 100 mm, respectively. The thickness of every rock sample was 50 mm, and the friction contact area of each side was 0.01 m^2. Quartz is the main content of granite which is widely distributed in natural fault zones. A number of previous researches directly used pure quartz powder as the infill material to study the fault mechanics (e.g., Boettcher and Marone 2004; Hong and Marone 2005; Kilgore et al. 2017; Marone and Saffer 2015). We used the commercial-available quartz powder as the simulated fault gouge with the mass of 35 g in each layer, and its purity of SiO_2 was no less than 99.5%. Quartz inhibits stick–slip under a relative low stress (Zhang et al. 2019), and stable sliding consistently occurs during the following friction tests. Figure 1c shows its grain size distribution as most particles were between 200 to 700 μm.

2.2 SHS tests

We conducted all the friction experiments in a room-humidity (around 75%) and room-temperature (around 15 °C) environment. These tests were displacement driven (referred by load point position). We consider two common stress levels $\sigma_n = 5$ and 7 MPa. The load point moved after the normal load is gradually applied to 5 MPa. First, we set a constant loading point velocity (v_{lp}) of 0.5 mm/min and a sliding distance of 2 mm for the run-in process (the shear load can reach the steady state). After that, the shear hold was executed at every 0.5 mm load point displacement for 3, 10, 30, 100, 300 and 1000 s during the whole process, and the first hold was started at 2 mm displacement. Next, the normal loading level was gradually increased to 7 MPa, and the previous experiment procedure was repeated. As a result, the final load point displacement was 10 mm.

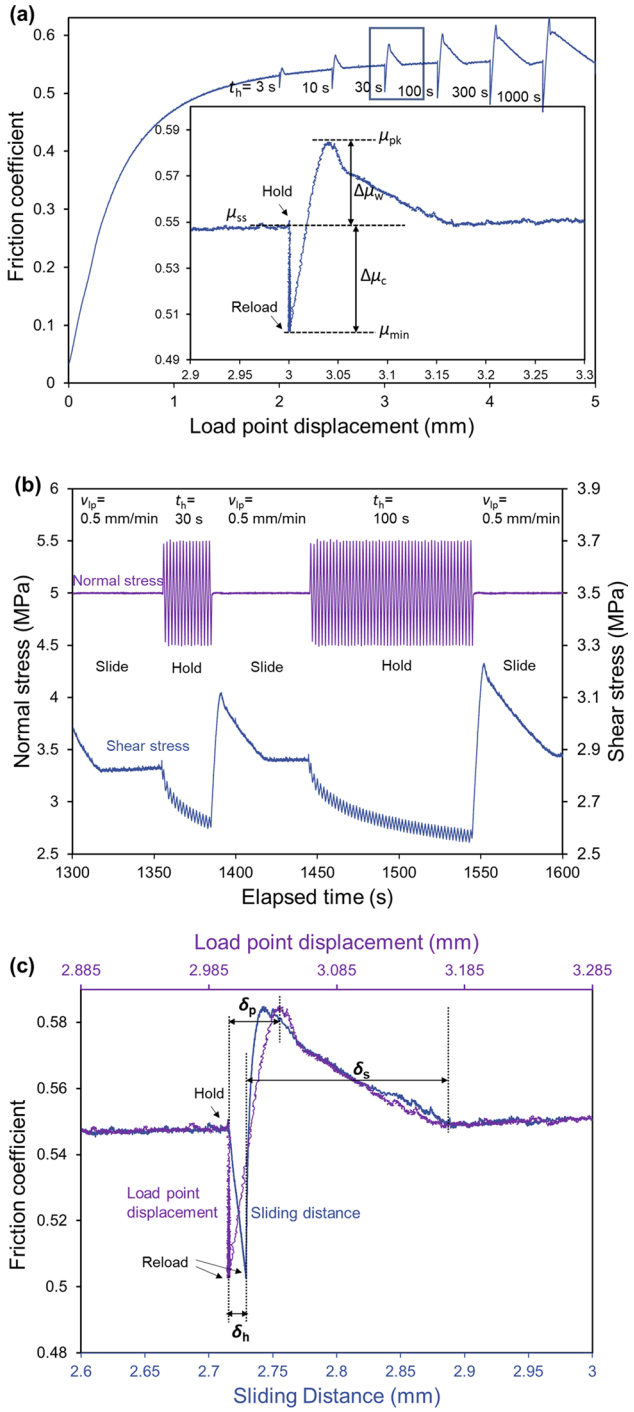

Fig. 3 Anatomy of SHS tests. **a** A typical SHS result (No. CH1) to derive the frictional healing ($\Delta\mu_w$) and frictional relaxation ($\Delta\mu_c$) based on the experimental data **b** Normal stress, load point displacement and shear stress response in a dynamic SHS test **c** Slip characteristics of fault during holding and the following sliding. δ_h is the creep length that occurs during the hold, up to the moment when the load point restarts. δ_p is the onward slip that occurs prior to peak friction, and is referred to as 'precursory slip'. δ_s is a measure of the slip necessary from reloading to reach the stable value of sliding friction

In the 'dynamic SHS tests', the σ_n oscillated as triangle waves during t_h. We set different wave amplitudes and frequencies in two test groups (Tests FH1–FH5, Test AH1–AH5) to simulate the dynamic stress disturbance in the fault zone, and the mean normal stress levels did not change. As summarized in Table 1, we conducted a SHS test (Test CH1) under consistent constant normal stress for comparison; Tests FH1–FH5 was concerning the effects of normal load oscillation frequency (f) from 0.1 to 1 Hz, and Test AH1–AH5 was concerning the effects of normal load oscillation amplitude from (ε) 5% to 25%. All the v_{lp} was kept at 0.5 mm/min during slide in this work.

3 Results and analysis

3.1 General features

Figure 2 reports the shear stress response as a function of load point displacement in the SHS test of the two stress levels. Figure 3 illustrates the important characteristics of the SHS test in this research. As shown in Fig. 3a, when the fault gouge slide to the specified distance, the loading piston stopped moving, and the friction can be observed to decrease continuously (the decreasing rate is fast at first and then slow). After the load point displacement had been maintained for a hold time (t_h), there was a peak value of friction after the reload, which was mostly higher than the steady-state friction (μ_{ss}) before the hold. After that, the friction coefficient dropped to reach a new steady-state value, which was similar to the friction before the last hold process. This behavior has been described as 'Dieterich-type' friction healing (Chen et al. 2015). Here, two parameters are generally needed to reflect this frictional evolution, namely, 'friction healing' and 'friction relaxation'. In other words, the difference between the μ_{ss} and the peak friction coefficient after the reload (μ_{pk}) is defined as friction healing ($\Delta\mu_w$) (Ikari et al. 2014; Carpenter et al. 2016b; Chen et al. 2015). Also, the friction relaxation ($\Delta\mu_c$) is calculated by subtracting the minimum friction coefficient during hold (μ_{min}) (usually at the moment before the load point moves again) from the μ_{ss}. Previous studies have shown that $\Delta\mu_w$ is controlled by t_h in a certain range and can be characterized by friction healing rate (β_w). As shown in the Eq. (1) and Figs. 4 and 5, if t_h is marked on a logarithmic x-axis, then $\Delta\mu_w$ is arranged in a straight line whose slope equals the frictional healing rate. Similarly, as formulated in Eq. (2), the frictional relaxation rate (β_c) follows the same logarithmic relation and can be calculated using the same method.

Faults can strengthen (heal) between earthquakes, and the rate of this healing process plays a key role in determining

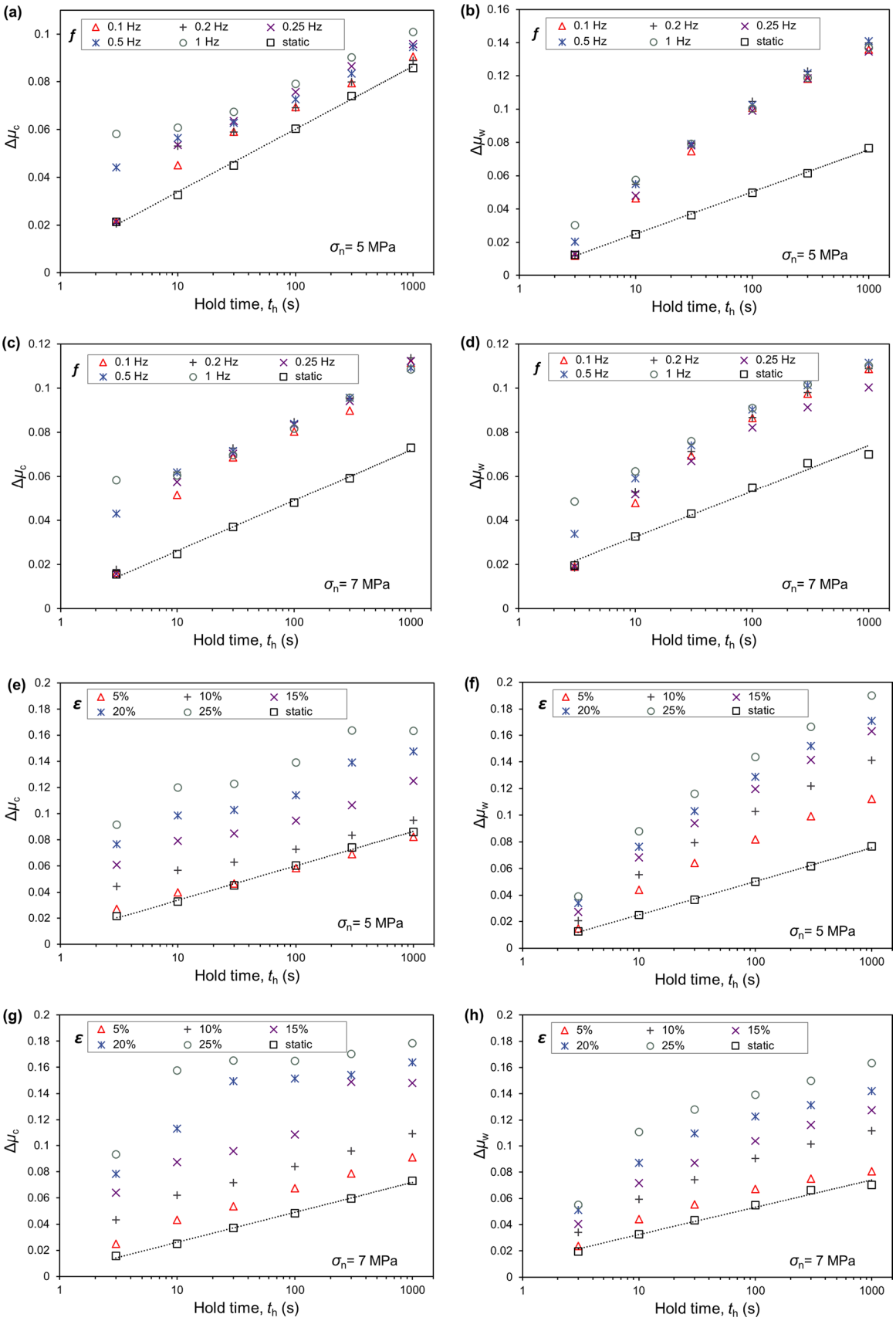
(a)
f
0.1 Hz
0.2 Hz
0.25 Hz
0.5 Hz
1 Hz
static
σ_n= 5 MPa
$\Delta\mu_c$
Hold time, t_h (s)
(b)
$\Delta\mu_w$
(c)
σ_n= 7 MPa
(d)
(e)
ε
5%
10%
15%
20%
25%
(f)
(g)
(h)

◂**Fig. 4** The results of relaxation and frictional healing considering different normal load oscillation frequencies during relaxation stage. **a** Frictional relaxation for different hold time under normal stress of 5 MPa **b** Frictional healing for different hold time under normal stress of 5 MPa **c** Frictional relaxation for different hold time under normal stress of 7 MPa **d** Frictional healing for different hold time under normal stress of 7 MPa. The results of creep relaxation and frictional healing considering different normal load oscillation amplitudes during relaxation stage **e** Frictional relaxation for different hold time under normal stress of 5 MPa **f** Frictional healing for different hold time under normal stress of 5 MPa g Frictional relaxation for different hold time under normal stress of 7 MPa h Frictional healing for different hold time under normal stress of 7 MPa

earthquake characteristics (Marone 1998b). The overserved $\Delta\mu_w$ in SHS test is considered the mechanism most likely to be responsible for natural fault strengthening. Higher β_w implies that the frictional strength which is necessary to prime fault re-rupture is fast recovered during interseismic period, with an important impact on repeated seismic cycles (Ikari et al. 2014). The frictional relaxation is a consequence of gouge creeping and is analogous to the after-slip in seismic cycles. It is a process to release the strain energy around the fault. As a result, the relaxation $\Delta\mu_c$ during a certain hold period is associated with earthquake after-slip behavior (Marone et al. 1991; Zhang et al. 2019).

$$\Delta\mu_w = \mu_{pk} - \mu_{ss} = \beta_w \cdot \log t_h \tag{1}$$

$$\Delta\mu_c = \mu_{ss} - \mu_{min} = \beta_c \cdot \log t_h \tag{2}$$

Moreover, as shown in Fig. 3b, in the tests FH1–FH5 and AH1–AH5 which include oscillatory normal stress during hold stages, in these holds, the fluctuation of normal stress will cause the fluctuation of shear stress, combing with the frictional descending trend similar to the conventional SHS test. For the variation patterns of sliding displacement, Fig. 3c show details of the friction coefficient as a function of two independent measurements of both fault sliding distance (based on the position of middle sliding block) and load point displacement (based on the position of vertical piston) during a 30 s hold (the insert in Fig. 3a). Two friction curves were drawn flowing these two x-axes. Due to finite shear stiffness, "Load point displacement" and "Sliding distance" are not equal. Note that during the hold period, the middle block was not absolutely stationary, but was 'creeping' at a low rate. Therefore, when the friction coefficient got its peak value, the corresponding displacements of the sliding block and the load point were not identical. Figure 3c tends to demonstrate slip characteristics of fault during holding and the following sliding. The real sliding velocity of the fault (creep rate) will be discussed in Sect. 4.1, and the δ_h is the slip (creep length) that occurs during the hold. Additionally, as marked in Fig. 3c, during reload, the μ_{pk} cannot be reached immediately, so there is a precursory slip of the load point (δ_p) prior to peak friction. And we found that the slip length required to reach μ_{ss} again from the μ_{pk}, i.e., δ_s, is also affected by the normal load oscillations.

3.2 Frictional strengthening and frictional relaxation

Figure 4a–d report the results of frictional relaxation and frictional healing of Test FH1–FH5 (considering different normal load oscillation frequencies during relaxation stage), and Fig. 4e–h report the results of frictional relaxation and frictional healing of Test AH1–AH5 (considering different normal load oscillation amplitudes during relaxation stage). As shown in Fig. 4a–d, compared to the static test, the value of $\Delta\mu_w$ and $\Delta\mu_c$ is larger in dynamic tests. However, among these tests, changing the oscillation frequency will not create a remarkable difference of the $\Delta\mu_w$ and $\Delta\mu_c$. As can be seen in Fig. 5a, the values of β_c are similar between static and dynamic results, and higher normal stress leads to higher β_c for dynamic tests. Besides, the oscillatory normal loads can enhance the magnitude of β_w (Fig. 5b), and higher normal stress leads to lower β_w for dynamic tests. The oscillation amplitude has an evident influence on $\Delta\mu_w$ and $\Delta\mu_c$. As shown in Fig. 4e–h, compared to the static test, the value of $\Delta\mu_w$ and $\Delta\mu_c$ consistently increased in every hold stage, and increasing the oscillation amplitudes will create remarkable enhancement of the $\Delta\mu_w$ and $\Delta\mu_c$ among these tests. After the intense normal load oscillation (Test AH4 and AH5), these linear relationships of $\Delta\mu_w$ or $\Delta\mu_c$ with $\log(t_h)$ are not perfectly regular. However, the values of β_c are still similar between static and dynamic results (Fig. 5c). Also, β_w at 5 MPa consistently greater than β_w at 7 MPa, and β_w increased significantly and uniformly as the amplitude increased (Fig. 5d).

3.3 Frictional response during normal oscillations

As mentioned in Sect. 3.1, in the relaxation stage, the fluctuation of normal force will cause gentle fluctuation of frictional stress. Figure 6a shows the variation pattern of shear stress and apparent friction coefficient (real-time shear stress divided by real-time normal stress) since the beginning of 1000 s hold in the Test AH5. As can be seen, the increase and decrease of shear stress function and normal stress function are consistent, and there is no phase difference between them. This is different from the phenomenon in the stable sliding on fault gouge or bare fractures (Dang et al. 2021, 2022a, 2022b). However, the increase and decrease of the apparent friction coefficient function and the normal stress

function are completely opposite, so the phase difference between them always equals half of the period.

Figure 6b reports the variation of friction coefficient (peak to valley) with different oscillation frequencies and amplitudes. Varying the oscillation frequency of normal load does not change the variation magnitude of apparent friction coefficient. However, the variation of the apparent friction coefficient in a cycle is proportional to the amplitude of the oscillatory normal load. We also calculated the shear loading rate as a function of normal loading rate. As shown in Fig. 6c, the shear loading rate is also proportional to the normal loading rate, and both increase synchronously in the two groups of experiments. However, as shown in Fig. 6d, the corresponding variation proportion is weak, with only around 4.5% of the magnitude of the normal effect.

3.4 Normal deformation

The dilation or compaction normal to the sliding plane also play an important role in the seismic cycles combining with the relaxation and strengthening processes (Marone 1998b; Ikari et al. 2009; Marone and Saffer 2015; Carpenter et al. 2016b; Zhang et al. 2019). Because of the much greater Young's modulus of the granite matrix, almost normal deformation during the test originated from the infilled gouge. We analyzed the normal deformation patterns (total deformation concluding two layers) of the gouge layer when $\sigma_n = 5$ MPa, and reported the results in Fig. 7. In all the tests, continuous shearing resulted in significant compaction and it contributed to the increase of shear stress. In addition to the compaction due to the shear motion, some part of compaction of the layer was also obtained during static contact (shown in Fig. 7). In the SHS test, the layer is always compacted during the hold, and existing works showed that layer compaction proceeds roughly linearly with log hold time in SHS tests (Marone and Saffer 2015; Carpenter et al. 2016b).

In this work, we focus on the normal deformation variation that happened in the hold period. As shown in Fig. 8a, under the oscillatory normal load, the gouge layers were compressed and released periodically, so the normal displacement curves also follow the term of triangular wave. The normal displacement variation during one load cycle

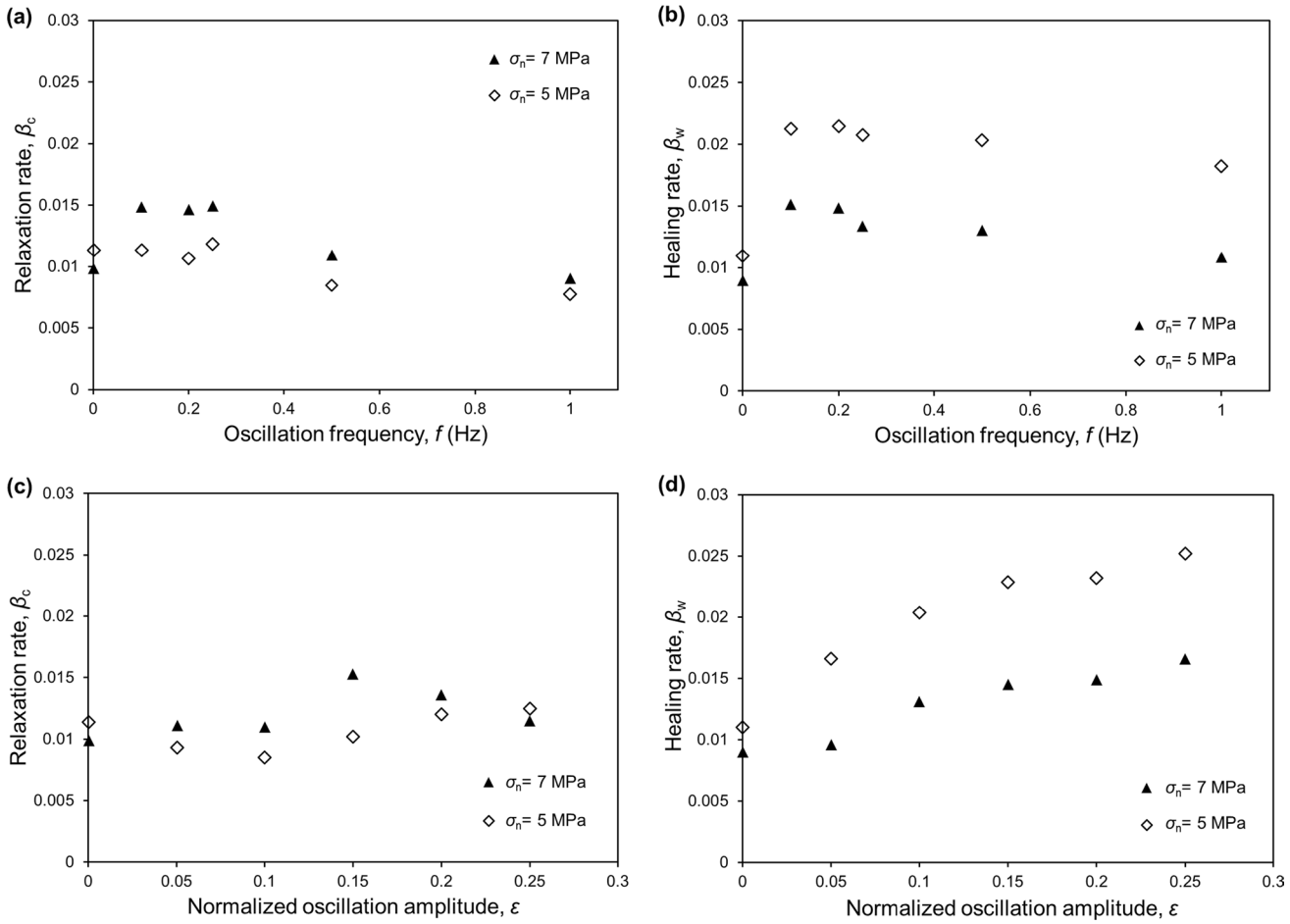

Fig. 5 The calculated relaxation rate and healing rate under two normal stress levels. **a**, **b** Test FH1–FH5 **c**, **d** Test AH1–AH5

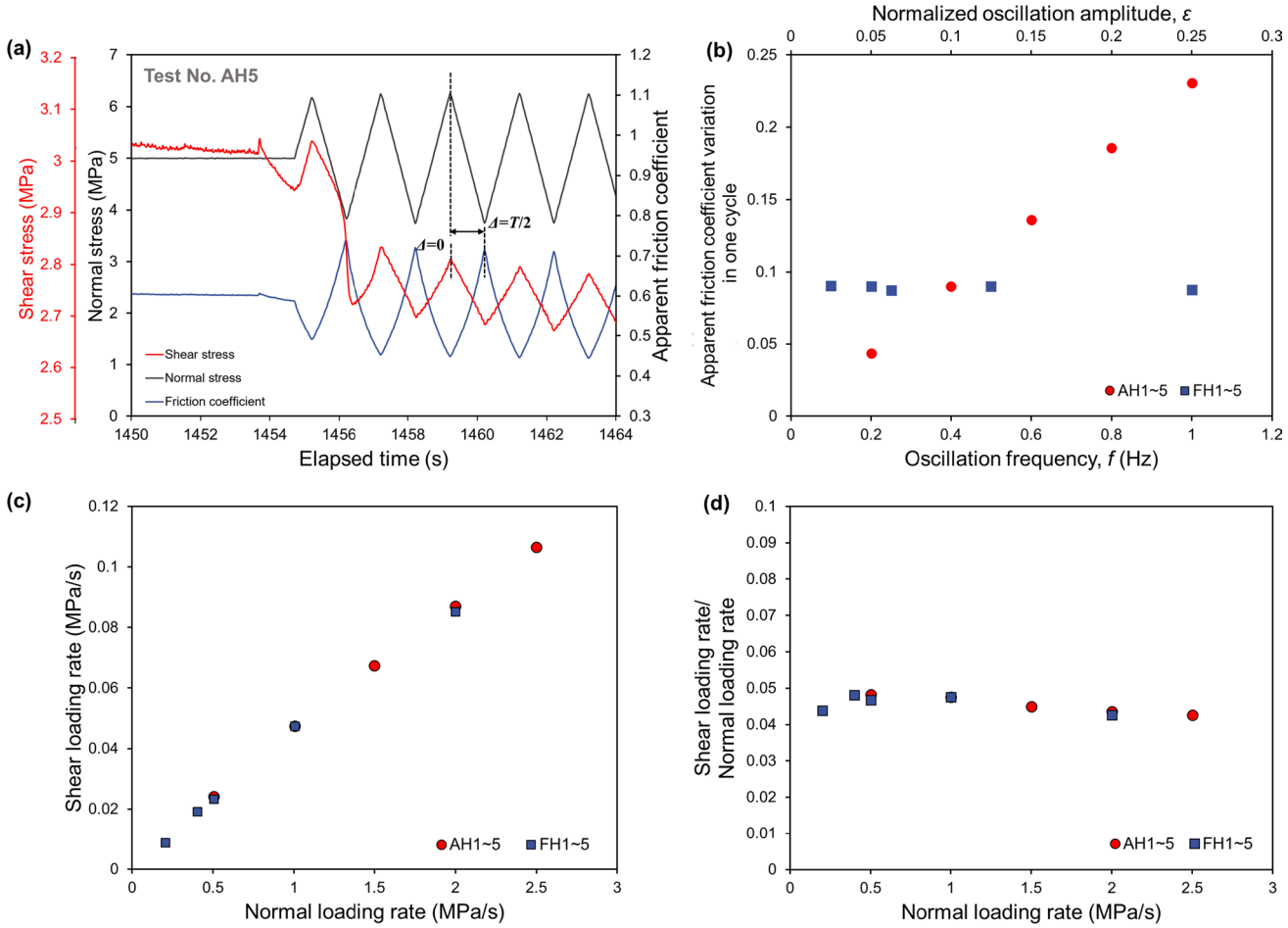

Fig. 6 The frictional response induced by normal load oscillation during holding stage. **a** An example of shear stress and apparent friction coefficient variation in the holding stage (1000 s hold) **b** Variation of friction coefficient (peak to valley) with different oscillation frequencies and amplitudes **c** The shear loading rate as a function of normal loading rate **d** The shear load response sensitivity (shear loading rate divided by normal loading rate) as a function of normal loading rate

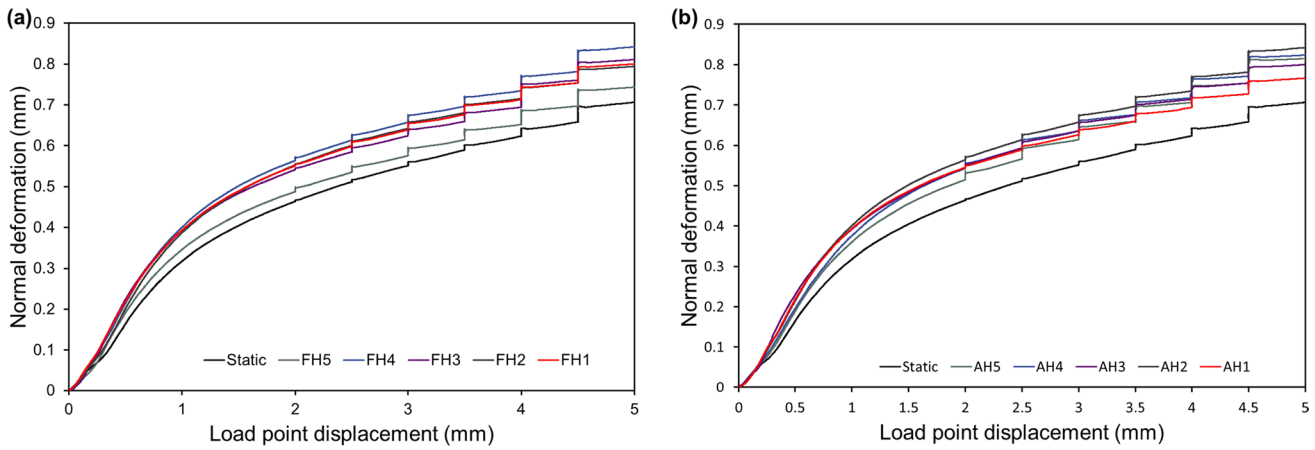

Fig. 7 Normal deformation of the whole shear process when $\sigma_n = 5$ MPa. **a** Test FH1–FH5 **b** Test AH1–AH5

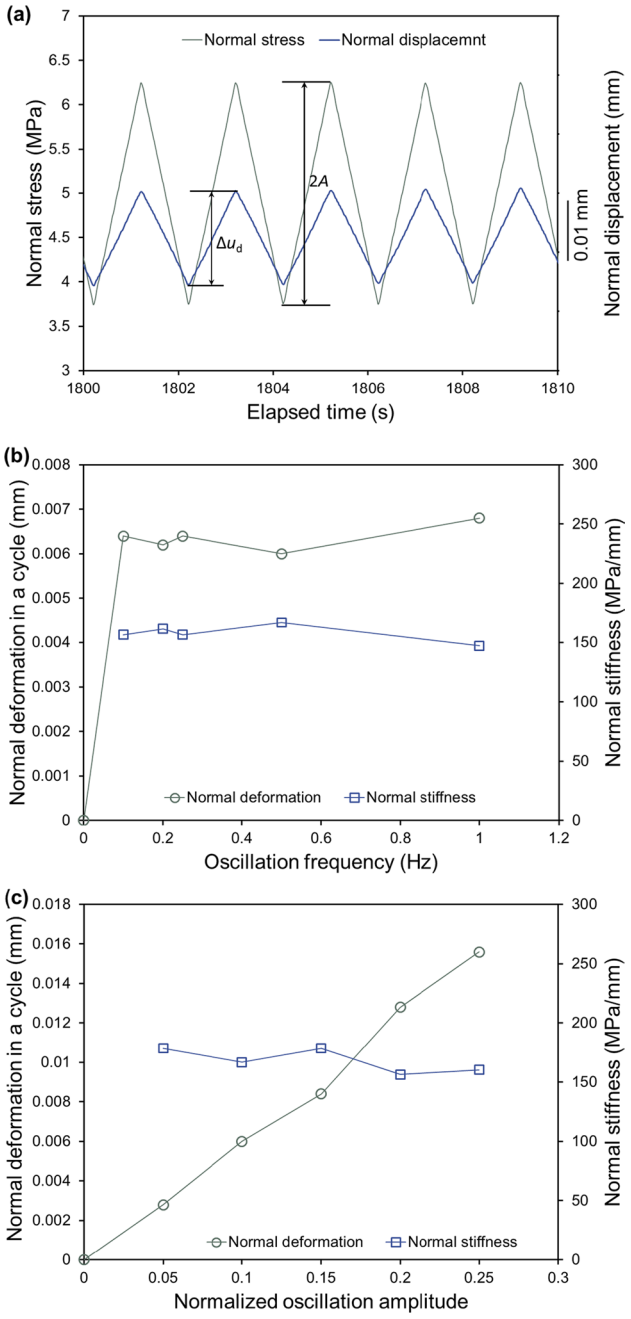

Fig. 8 **a** Normal displacement variation effected by oscillatory normal load in hold stage; the characteristics of cyclic normal deformation considering **b** Normal load oscillation frequency and **c** Oscillation amplitude, which includes the normal deformation in a load cycle during 300 s hold under the normal load of 5 MPa and the calculated normal stiffness

(Δu_d) remains basically unchanged, and there is no phase lag between the normal stress and the normal displacement. Moreover, the change of layer thickness can be considered as a restorable deformation in a short time span, so the normal stiffness of the layer can be calculated as $\Delta u_d/2A$. As shown in Fig. 8b, Δu_d does not experience a significant change when normal load oscillation frequency varies; in Fig. 8c, Δu_d increases linearly with the increase of oscillation amplitude. So the normal stiffness of the quartz layer nearly keeps a constant of around 160 MPa/mm under different loading conditions.

4 Discussion

4.1 Creep and precursory slip

Figures 9 and 10 present the slip characteristics (creep during the hold and the precursory slip δ_p after reload) under two stress levels. The slip patterns under 5 and 7 MPa normal stresses are similar. During the hold stage, the sliding surfaces were still creeping at a very low rate although the loading point was stationary. As shown in Fig. 9a, c, for different normal load oscillation frequencies, the creep rate decreases with the increase of holding time, and the logarithm of the two variables shows nearly linear relations in the plots. Also, there is no obvious distinction between the static and the dynamic tests. As shown in Fig. 10a, c, for different oscillation amplitudes, the creep patterns are similar, and the difference between the static and dynamic tests are also not obvious. The precursory slip is an essential parameter in fault friction (Johnson 1981; Acosta et al. 2019; Cattania and Segall 2021). Similarly, the effect of normal stress level is minor. As shown in Fig. 9b, d, the δ_p can also scale with hold time by a logarithmic linear relationship. However, this linear trend cannot be kept when the oscillation amplitude is large (Fig. 10b, d). From the two sets of dynamic tests, we can see that the oscillatory normal load will increase the magnitude of δ_p. Meanwhile, the δ_p consistently increases when the normalized oscillation amplitude is larger, but δ_p does not shown much difference when adjusting normal load oscillation frequency.

4.2 Delayed steady state

As can be seen in Fig. 3, the evolution of after-peak friction coefficient shows a decrease until it reaches the μ_{ss} again. The residual slip (δ_s) in Fig. 3c is the slip necessary to reestablish steady sliding, i.e., the slip at which friction-displacement curves become flat again. Previous researches reported the δ_s seems to scale with hold time, too (Marone and Saffer 2015). As shown in Fig. 11, we found that compared to conventional SHS tests, the average descending rates of friction coefficient (the main slope of the friction curves after peak) are much lower, causing that the return to frictional steady state is delayed (the δ_s will be longer). As shown in Fig. 11a, the descending rates do not experience an obvious change

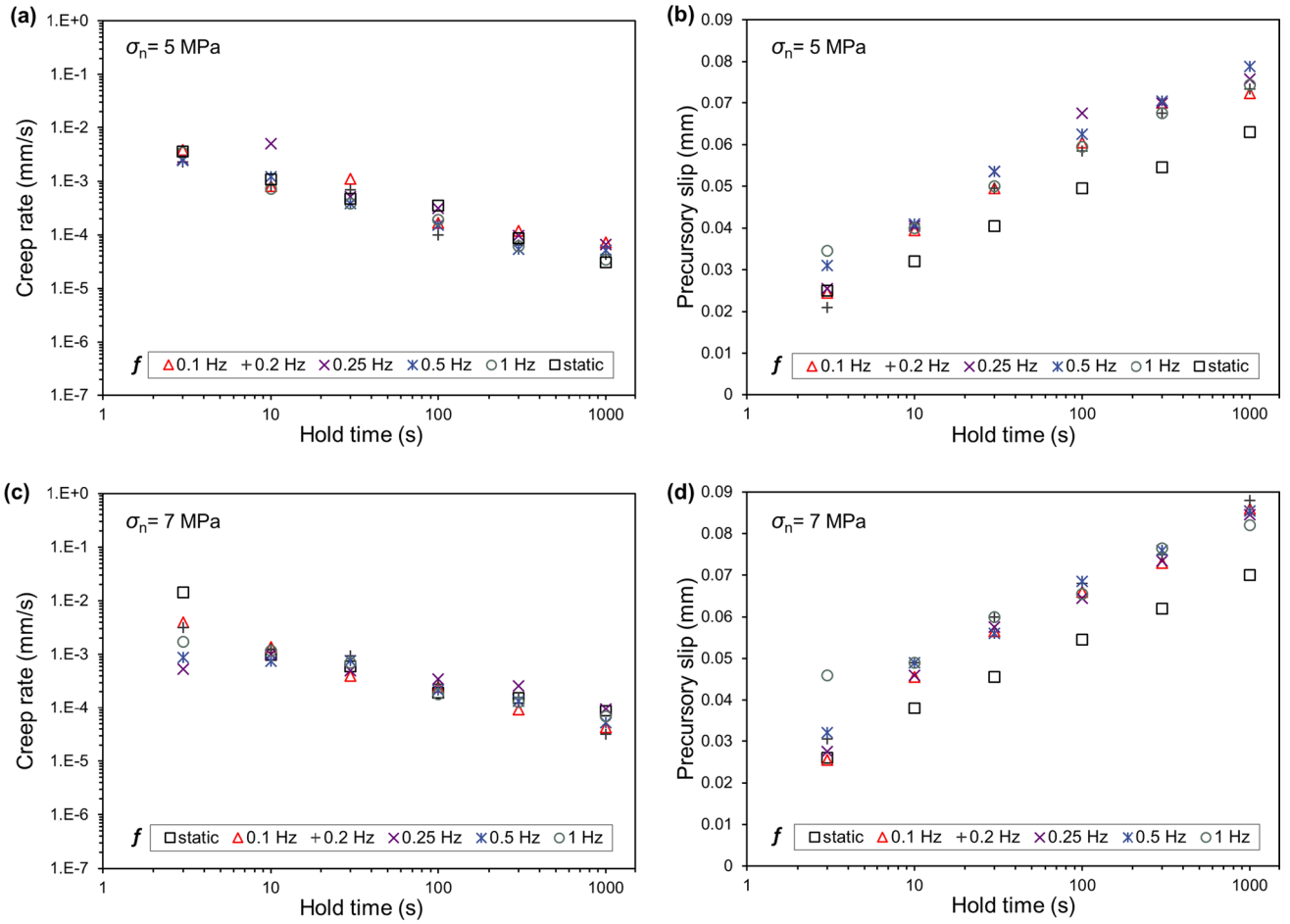

Fig. 9 Details of relaxation creep rate and precursory slip length in SHS tests considering different normal load oscillation frequencies during relaxation stage. **a** Creep rate for different hold time under normal stress of 5 MPa **b** Precursory slip length for different hold time under normal stress of 5 MPa **c** Creep rate for different hold time under normal stress of 7 MPa **d** Precursory slip length for different hold time under normal stress of 7 MPa

when the frequency of oscillatory normal load during hold increases. However, as shown in Fig. 11b, by improving the oscillation amplitude, the rate of friction decreasing reduces consistently, causing a longer distance to reach μ_{ss}.

When explaining the larger $\Delta\mu_w$, $\Delta\mu_c$ and friction descending rate in the dynamic tests, this result is potentially caused by the rearrangement of the gouge particles owning to the oscillatory normal stress. Generally, frictional healing is the process that the faults regain the shear strength through the increase of micro-contact area (Ikari et al. 2014). During last hold, the crushed mineral particles bond together through the normal compression and the number particle–particle contact points increased (Jia et al. 2022). As the normal deformation increases linearly with the increase of ε (Fig. 8), consequently, larger ε causes larger $\Delta\mu_w$. However, the normal deformation does not experience a significant change when f varies, indicating that changing the f will not create a remarkable difference of the $\Delta\mu_w$. Similarly, the gouge was more strengthened through the increase of micro-contact area because of oscillatory σ_n in hold period, causing the longer δ_s. And f has a minor effect because the micro-contact condition is stable with same oscillation amplitude. As for frictional relaxation, the hold periods are processes to release the strain energy stored in the shear system and cause shear load reductions (Marone 1991). The energy is faster released when normal load is more dramatically unloaded, hence larger ε causing larger $\Delta\mu_c$.

5 Conclusions

To explore the effects of varied normal load on the fault friction during interseismic period, dynamic slide-hold-slide (SHS) tests on quartz gouge were performed. We used oscillatory normal stress considering different normal load oscillation frequency and amplitude during the quasi-stationary contact (hold) process.

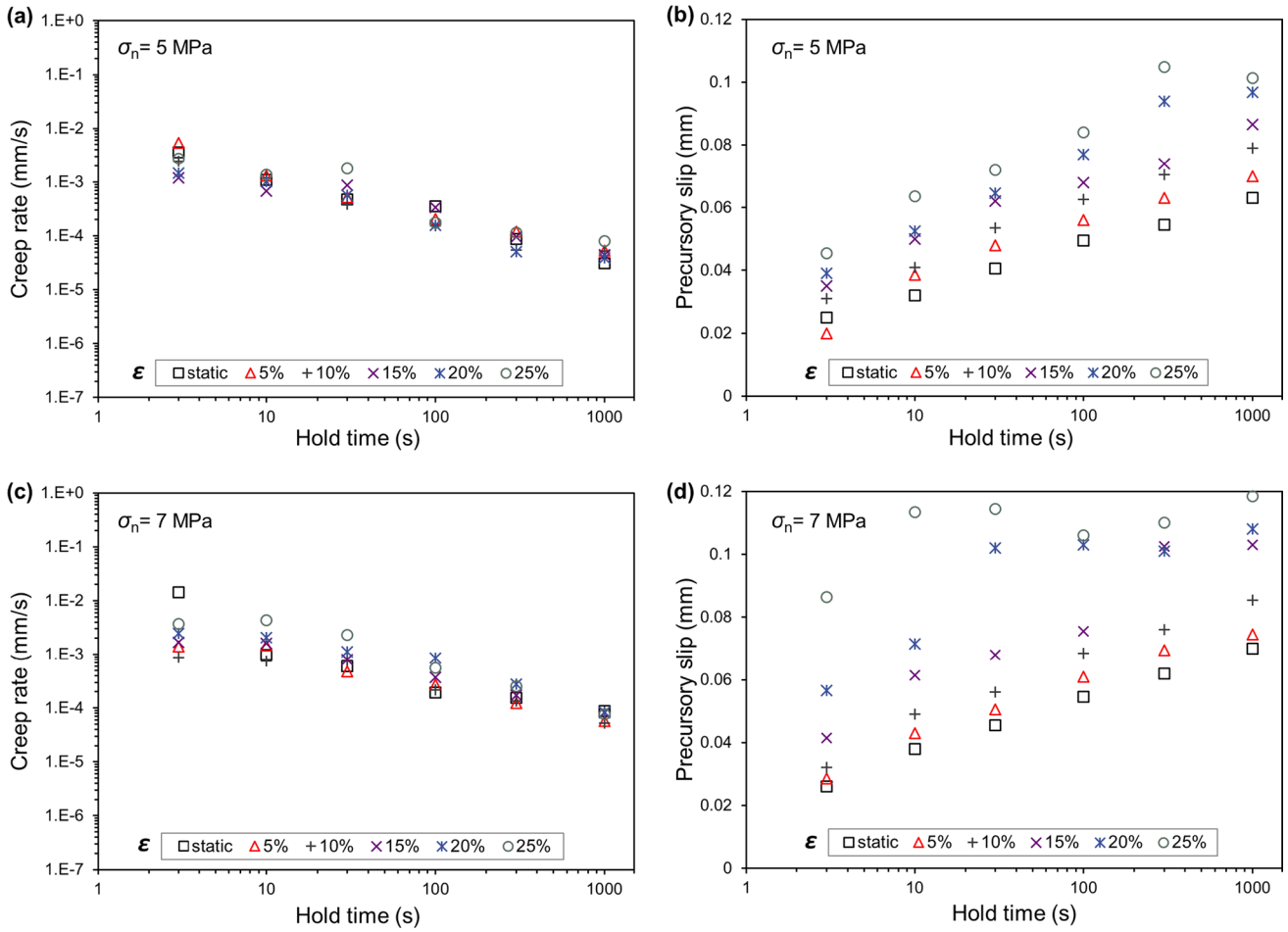

Fig. 10 Details of relaxation creep rate and precursory slip length in SHS tests considering different normal load oscillation amplitudes during relaxation stage. **a** Creep rate for different hold time under normal stress of 5 MPa **b** Precursory slip length for different hold time under normal stress of 5 MPa **c** Creep rate for different hold time under normal stress of 7 MPa **d** Precursory slip length for different hold time under normal stress of 7 MPa

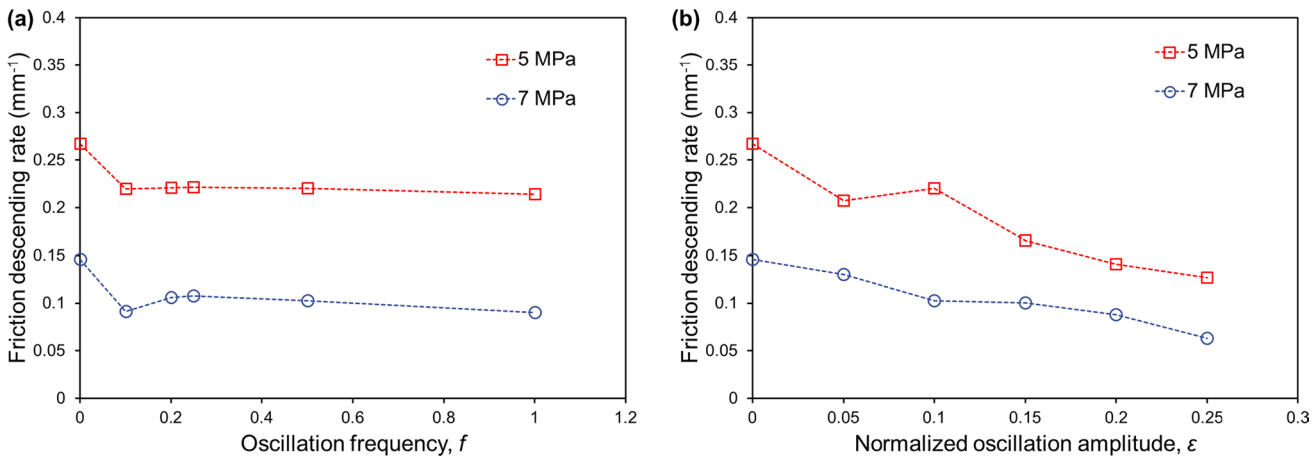

Fig. 11 The post-peak slope (the rate of friction descending) which demonstrates the delayed steady state as a function of **a** Normal load oscillation frequency and **b** Normalized normal load oscillation amplitude

During hold stages, the fluctuation of normal stress will cause the fluctuation of shear stress, combing with the frictional descending trend similar to the conventional SHS test. The normal load oscillation amplitude can make a positive effect on the relaxation and healing characteristics. Both the magnitude of frictional relaxation and frictional healing consistently increase with larger oscillation amplitude, and the rate of frictional healing increases uniformly when improving the oscillation amplitude. But the frictional relaxation rate is not notably affected by the oscillation amplitude under two stress levels. All of these characteristics do not experience an obvious evolution when changing the normal load oscillation frequency. Besides, during the process of relaxation, the shear stress fluctuates synchronously with the normal stress, the shear loading rate is proportional to the normal loading rate, and the normal stiffness of the quartz layer nearly keeps a constant under different normal loading conditions. During the hold stage, the sliding surfaces are still creeping at a very low rate, which shows no obvious distinction between the static test and the dynamic tests. The precursory slip also scales with hold time by a logarithmic linear relationship, and it is increased by larger oscillation amplitude. Compared to conventional SHS tests, the descending rates of friction coefficient in the dynamic tests are much lower, causing the delayed return to frictional steady state.

In the current study, the mineral contents and initial thickness of gouge kept the same, so these factors will be studied in the future. Besides, we will upgrade our apparatus with dual syringe pumps so that the dynamic hydraulic effects (Ji et al. 2022; Ma et al. 2022) on faults healing will be explored.

Acknowledgements This research is financially supported by Fundamental Research Funds for the Central Universities (22dfx06) and Natural Science Foundation of Guangdong Province-Joint Program for Offshore Wind Power (2022A1515240009). The first author sincerely thanks Mr. Junpeng Chen and Mr. Xinfan Chen for their kind supports.

Author contributions Conceptualization, K.T. and W.D.; Methodology, K.T.; Formal analysis, K.T.; Investigation, K.T.; Resources, W.D.; Data curation, K.T. and W.D.; Writing—original draft preparation, K.T.; Writing—review and editing, K.T. and W.D.; Supervision, W.D.; Project administration, W.D.; Funding acquisition, W.D. All authors read and approved the final manuscript.

Data availability Data is available upon reasonable request to the corresponding author.

Declarations

Conflict of interest The authors declare that they have no conflict of interest.

References

Acosta M, Passelègue FX, Schubnel A, Madariaga R, Violay M (2019) Can precursory moment release scale with earthquake magnitude? A view from the laboratory. Geophys Res Lett 46:12927–12937

Beeler NM, Thomas A, Bürgmann R, Shelly D (2018) Constraints on friction, dilatancy, diffusivity, and effective stress from low-frequency earthquake rates on the deep San Andreas Fault. J Geophys Res Solid Earth 123(1):583–605

Beroza G, Ide S (2011) Slow earthquakes and non-volcanic tremor. Annu Rev Earth Planet Sci 39:271–296

Blanpied ML, Lockner DA, Byerlee JD (1995) Frictional slip of granite at hydrothermal conditions. J Geophys Res 100(B7):13045–13064

Boettcher MS, Marone, (2004) Effects of normal stress variation on the strength and stability of creeping faults. J Geophys Res Solid Earth 109(B3):B03406

Bürgmann R (2018) The geophysics, geology and mechanics of slow fault slip. Earth Planet Sci Lett 495:112–134

Carpenter BM, Collettini C, Viti C, Cavallo A (2016a) The influence of normal stress and sliding velocity on the frictional behaviour of calcite at room temperature: Insights from laboratory experiments and microstructural observations. Geophys J Int 205:548–561

Carpenter BM, Ikari MJ, Marone C (2016b) Laboratory observations of time-dependent frictional strengthening and stress relaxation in natural and synthetic fault gouges. J Geophys Res Solid Earth 121:1183–1201

Carpenter BM, Marone C, Saffer DM (2011) Weakness of the San Andreas fault revealed by samples from the active fault zone. Nature Geosci 4(4):251–254

Cattania C, Segall P (2021) Precursory slow slip and foreshocks on rough faults. J Geophys Res Solid Earth 126:e2020JB020430

Chen B (2020) Stress-induced trend: the clustering feature of coal mine disasters and earthquakes in China. Int J Coal Sci Technol 8(1):77–87

Chen J, Verberne BA, Spiers CJ (2015) Interseismic re-strengthening and stabilisation of carbonate faults by "non-Dieterich" healing under hydrothermal conditions. Earth Planet Sci Lett 423:1–12

Collettini C, Tesei T, Scuderi M, Carpenter B, Viti C (2019) Beyond Byerlee friction, weak faults and implications for slip behavior. Earth Planet Sci Lett 519:245–263

Dang WG, Chen JP, Huang LC (2021) Experimental study on the velocity-dependent frictional resistance of a rough rock fracture exposed to normal load vibrations. Acta Geotech 16:2189–2202

Dang WG, Tao K, Chen XF (2022a) Frictional behavior of planar and rough granite fractures subjected to normal load oscillations of different amplitudes. J Rock Mech Geotech Eng 14:746–756

Dang WG, Tao K, Huang LC, Li X, Ma JJ, Zhao TTG (2022b) A new multi-function servo control dynamic shear apparatus for geomechanics. Measurement 187:110345

Dang WG, Wang CP, Huang HL, Tao K, Ma JJ, Liang Y, Li X (2022) A novel three-directional servo control dynamic loading apparatus for geomechanics. Geomech Geophys Geo-energ Geo-resour 8(6):209

Das S, Aki K (1977) A numerical study of two-dimensional spontaneous rupture propagation. Geophys J Int 50:643–668
Delorey AA, van der Elst NJ, Johnson PA (2017) Tidal triggering of earthquakes suggests poroelastic behavior on the San Andreas Fault. Earth Planet Sci Lett 460:164–170
Dieterich JH (1972) Time-dependent friction in rocks. J Geophys Res 77:3690–3697
Dieterich JH, Kilgore BD (1994) Direct observation of frictional contacts: new insights for state-dependent properties. Pure Appl Geophys 143:283–302
Fan C, Liu J, Hunfeld LB, Spiers CJ (2020) Frictional slip weakening and shear-enhanced crystallinity in simulated coal fault gouges at slow slip rates. Solid Earth 11:1399–1422
Fang Y, Elsworth D, Ishibashi T, Zhang F (2018) Permeability evolution and frictional stability of fabricated fractures with specifed roughness. J Geophys Res Solid Earth 123:9355–9375
Foulger GR, Wilson MP, Gluyas JG, Julian BR, Davies RJ (2018) Global review of human-induced earthquakes. Earth-Sci Rev 178:438–514
Harris R (2017) Large earthquakes and creeping faults. Rev Geophys 55:169–198
Hong T, Marone C (2005) Effects of normal stress perturbations on the frictional properties of simulated faults. Geochem Geophys Geosyst 6:Q03012
Ide S, Beroza GC, Shelly DR, Uchide T (2007) A scaling law for slow earthquakes. Nature 447:76–79
Ikari MJ, Carpenter BM, Kopf AJ, Marone C (2014) Frictional strength, rate-dependence, and healing in DFDP-1 borehole samples from the Alpine Fault, New Zealand. Tectonophysics 630:1–8
Ikari MJ, Safer DM, Marone C (2009) Frictional and hydrologic properties of clay-rich fault gouge. J Geophys Res Solid Earth 114:B05409
Im K, Elsworth D, Marone C, Leeman J (2017) The impact of frictional healing on stick-slip recurrence interval and stress drop: Implications for earthquake scaling. J Geophys Res Solid Earth 122:10102–10117
Ji Y, Hofmann H, Duan K, Zang A (2022) Laboratory experiments on fault behavior towards better understanding of injection-induced seismicity in geoenergy systems. Earth-Sci Rev 226:103916
Jia Y, Song C, Liu R (2022) The Frictional restrengthening and permeability evolution of slipping shale fractures during seismic cycles. Rock Mech Rock Eng 55:1791–1805
Johnson T (1981) Time-dependent friction of granite: Implications for precursory slip on faults. J Geophys Res 86(B7):6017–6028
Kilgore B, Beeler NM, Lozos J, Oglesby D (2017) Rock friction under variable normal stress. J Geophys Res Solid Earth 122:7042–7075
Li LP, Zhang HT, Pan YS, Ju XY, Tang L, Li M (2022) Influence of stress wave-induced disturbance on ultra-low friction in broken blocks. Int J Coal Sci Technol 9:22
Ma D, Duan HY, Zhang JX, Bai HB (2022) A state-of-the-art review on rock seepage mechanism of water inrush disaster in coal mines. Int J Coal Sci Technol 9:50
Marone C (1991) A note on the stress-dilatancy relation for simulated fault gouge. Pure Appl Geophys 137(4):409–419
Marone C (1998a) Laboratory-derived friction laws and their application to seismic faulting. Annu Rev Earth Planet Sci 26(1):643–696
Marone C (1998b) The effect of loading rate on static friction and the rate of fault healing during the earthquake cycle. Nature 101(6662):1143–1152
Marone C, Saffer DM (2015) The mechanics of frictional healing and slip instability during the seismic cycle. In: Schubert G (ed) Treatise on geophysics, 2nd edn. Elsevier, Netherlands, pp 111–138
McLaskey GC, Thomas AM, Glaser SD, Nadeau RM (2012) Fault healing promotes high-frequency earthquakes in laboratory experiments and on natural faults. Nature 491:101–104
Montgomery DR, Jones DL (1992) How wide is the Calaveras fault zone? Evidence for distributed shear along a major fault in central California. Geology 20:55–58
Saffer DM, Marone C (2003) Comparison of smectite- and illite-rich gouge frictional properties: Application to the updip limit of the seismogenic zone along subduction megathrusts. Earth Planet Sci Lett 215(1–2):219–235
Unsworth M, Malin P, Egbert G, Booker J (1997) Internal structure of the San Andreas fault at Parkfield, CA. Geology 25:359–362
van der Elst NJ, Savage HM (2015) Frequency dependence of delayed and instantaneous triggering on laboratory and simulated faults governed by rate-state friction. J Geophys Res Solid Earth 120(5):3406–3429
Verberne BA, Niemeijer AR, De Bresser JHP, Spiers CJ (2015) Mechanical behavior and microstructure of simulated calcite fault gouge sheared at 20–600 °C: Implications for natural faults in limestones. J Geophys Res Solid Earth 120:8169–8196
Violay M, Giorgetti C, Cornelio C, Aeschiman F, Stefano GD, Gastaldo L, Wiemer S (2021) HighSTEPS: A high strain temperature pressure and speed apparatus to study earthquake mechanics. Rock Mech Rock Eng 54:2039–2052
Vlek C (2018) Induced earthquakes from long-term gas extraction in Groningen, the Netherland: statistical analysis and prognosis for acceptable-risk regulation. Risk Anal 38(7):1455–1473
Xu N, Li T, Dai F, Zhang R, Tang C, Tang L (2016) Microseismic monitoring of strainburst activities in deep tunnels at the Jinping II hydropower station. China Rock Mech Rock Eng 49(3):981–1000
Zhang F, An M, Zhang L, Fang Y, Elsworth D (2019) The role of mineral composition on the frictional and stability properties of powdered reservoir rocks. J Geophys Res Solid Earth 124:1480–1497
Zhang K, Li HF, Han JM, Jiang BB, Gao J (2021) Understanding of mineral change mechanisms in coal mine groundwater reservoir and their influences on effluent water quality: An experimental study. Int J Coal Sci Technol 8:154–167